International Journal of Nanomedicine

Dovepress
open access to scientific and medical research

Open Access Full Text Article

ORIGINAL RESEARCH

Graphene oxide scaffold accelerates cellular proliferative response and alveolar bone healing of tooth extraction socket

This article was published in the following Dove Press journal:
International Journal of Nanomedicine
24 May 2016
Number of times this article has been viewed

Erika Nishida[1]
Hirofumi Miyaji[1]
Akihito Kato[1]
Hiroko Takita[2]
Toshihiko Iwanaga[3]
Takehito Momose[1]
Kosuke Ogawa[1]
Shusuke Murakami[1]
Tsutomu Sugaya[1]
Masamitsu Kawanami[1]

[1]Department of Periodontology and Endodontology, Hokkaido University Graduate School of Dental Medicine, Sapporo, Japan; [2]Support Section for Education and Research, Hokkaido University Graduate School of Dental Medicine, Sapporo, Japan; [3]Laboratory of Histology and Cytology, Hokkaido University Graduate School of Medicine, Sapporo, Japan

Abstract: Graphene oxide (GO) consisting of a carbon monolayer has been widely investigated for tissue engineering platforms because of its unique properties. For this study, we fabricated a GO-applied scaffold and assessed the cellular and tissue behaviors in the scaffold. A preclinical test was conducted to ascertain whether the GO scaffold promoted bone induction in dog tooth extraction sockets. For this study, GO scaffolds were prepared by coating the surface of a collagen sponge scaffold with 0.1 and 1 μg/mL GO dispersion. Scaffolds were characterized using scanning electron microscopy (SEM), physical testing, cell seeding, and rat subcutaneous implant testing. Then a GO scaffold was implanted into a dog tooth extraction socket. Histological observations were made at 2 weeks postsurgery. SEM observations show that GO attached to the surface of collagen scaffold struts. The GO scaffold exhibited an interconnected structure resembling that of control subjects. GO application improved the physical strength, enzyme resistance, and adsorption of calcium and proteins. Cytocompatibility tests showed that GO application significantly increased osteoblastic MC3T3-E1 cell proliferation. In addition, an assessment of rat subcutaneous tissue response revealed that implantation of 1 μg/mL GO scaffold stimulated cellular ingrowth behavior, suggesting that the GO scaffold exhibited good biocompatibility. The tissue ingrowth area and DNA contents of 1 μg/mL GO scaffold were, respectively, approximately 2.5-fold and 1.4-fold greater than those of the control. Particularly, the infiltration of ED2-positive (M2) macrophages and blood vessels were prominent in the GO scaffold. Dog bone-formation tests showed that 1 μg/mL GO scaffold implantation enhanced bone formation. New bone formation following GO scaffold implantation was enhanced fivefold compared to that in control subjects. These results suggest that GO was biocompatible and had high bone-formation capability for the scaffold. The GO scaffold is expected to be beneficial for bone tissue engineering therapy.

Keywords: biocompatibility, biomaterial, bone tissue engineering, cell ingrowth, collagen sponge, macrophage, nanocarbon

Introduction

Tissue engineering therapy, which is intended to reconstruct tissues lost because of destructive diseases such as inflammation and tumors, requires three major elements: cells, signaling molecules, and scaffolds.[1,2] Many investigators have developed natural and artificial three-dimensional (3D) scaffolds for tissue engineering of various tissues. The scaffolds provide the field and space for retaining growth and nutrition factors to facilitate the repopulation and differentiation of stem cells,[3] blood vessels, and extracellular matrices.[4,5] Recently, scaffolds used in combination with stem cell seeding and growth factor application were helpful for tissue regeneration.[6,7] Therefore, refinement

Correspondence: Hirofumi Miyaji
Department of Periodontology and Endodontology, Hokkaido University Graduate School of Dental Medicine, N 13 W 7, Kita-ku, Sapporo 060-8586, Japan
Tel +81 11 706 4266
Fax +81 11 706 4334
Email miyaji@den.hokudai.ac.jp

submit your manuscript | www.dovepress.com
Dovepress
http://dx.doi.org/10.2147/IJN.S104778

of the scaffold specifications for regenerative medicine is anticipated for upregulating bioactive properties in clinical use, including the self-assembly of compound tissues and organs. To improve scaffold therapy efficiency, nanosized substances have been used in recent times as regenerative biomaterials. The nanostructured surfaces of biomaterials have greatly increased the surface area to achieve high roughness and wettability.[8,9] Moreover, nanostructures formed on regenerative devices greatly promote biological behaviors such as cell adhesion, migration, proliferation, and differentiation.[10–12] Accordingly, nanotechnology related to tissue engineering therapy is expected to be useful as a contribution to scaffold biologic development and to physiologic improvements.

Carbon-based nanosubstrates, such as carbon nanotubes,[13,14] carbon nanohorns,[15] carbon nanofibers,[16] and graphene,[17,18] have been investigated widely for stem cell therapies and tissue engineering platforms because of their unique physical, chemical, and mechanical properties. Graphene oxide (GO) in a two-dimensional honeycomb lattice of a carbon monolayer is obtained by oxidation and exfoliation of graphite.[19] It exhibits high dispersibility[20] and hydrophilicity.[21] Particularly, the outstanding surface activity of GO, which is most likely caused by many functional groups on its surface, can exert adsorptive capability to drugs,[22,23] growth factors,[24] and other biomolecules[25] and can consequently provide important benefits related to tissue engineering therapy. In addition, several in vitro experiments have demonstrated that the use of GO markedly increased the degree of proliferation and differentiation of cultured cells, thereby suggesting that GO possesses good biocompatibility.[26–28] Dinescu et al[29] reported that the application of GO to the chitosan 3D scaffold stimulated the formation of the interconnected pore structure and enhanced the proliferative activity of attached cells. In addition, Wu et al[30] demonstrated that β-tricalcium phosphate scaffold modified with GO accelerated the formation of new bone compared to nonmodified scaffold in rabbit cranial bones. Therefore, nanomodification using GO might play a major role in providing excellent bioactivity to a regenerative scaffold and might promote subsequent biointegration between the scaffold and surrounding tissue during bone tissue engineering therapy.

The dosage of nanomaterial application is an important factor related to biocompatibility because high doses of nanomaterials frequently stimulate adverse effects following biomedical application. Huang et al[31] reported that the application of hydroxyapatite nanoparticles of less than 100 nm diameter with high concentration stimulated the attachment and growth of osteoblastic cells. However, lactate dehydrogenase production of macrophages was also induced, thereby suggesting the cytotoxicity of hydroxyapatite nanoparticles. Other reports have described that nanocarbon materials exhibit toxic effects on cell viability in a time- and dose-dependent manner. Bottini et al[32] reported that carbon nanotubes applied at markedly high concentrations can stimulate human T-cell apoptosis. Previously, we created a GO film on a culture dish and assessed the toxic dose effect of GO in association with the viability of cultured osteoblastic MC3T3-E1 cells. Results showed that proliferation and alkaline phosphatase activity of E1 cell decreased in a GO dose-dependent manner. In addition, GO application to a scaffold of Type I collagen promoted the mechanical properties of scaffold in a GO dose-dependent manner. However, the biocompatibility of GO-applied scaffold in rat connective tissue was consistently low at the loading of GO at higher doses (over 10 μg/mL).[28] Furthermore, several investigators have presented similar results demonstrating that GO cytotoxicity occurred in a dose-dependent manner.[33,34] Therefore, dose setting of GO, such as low dose of GO, is expected to play a key role in positive bioeffects and regenerative phenomena for biomedical applications.

This study was conducted to assess the cellular and tissue proliferative behaviors in relation to a GO scaffold when compared to untreated collagen scaffold in vitro and in vivo. Subsequently, we used preclinical tests to evaluate whether GO scaffold promotes bone induction in a dog tooth extraction socket or not.

Materials and methods

Fabrication and GO scaffold

A single-layer GO solution (nano GRAX®; Mitsubishi Gas Chemical Co. Inc., Tokyo, Japan) was prepared in water using the method described by Hummers and Offeman.[35] The GO monolayer thickness was less than 1 nm. Its average width was approximately 20 μm.[36] Subsequently, GO was dispersed in 1-methyl-2-pyrrolidinone (Wako Pure Chemical Industries Ltd., Osaka, Japan) to prepare 0.1 and 1 μg/mL GO dispersion. Then, 100 μL of each GO dispersion was injected into a 3D collagen sponge-form scaffold (6×6×3 mm, Terudermis®; Olympus Terumo Biomaterials Corporation, Tokyo, Japan) using a syringe with a 25-gauge needle. After rinsing several times with ethanol to remove the dispersion solution followed by subsequent air-drying, GO scaffolds were obtained for evaluation (Figure 1A). The collagen scaffold without GO modification was also assessed as control.

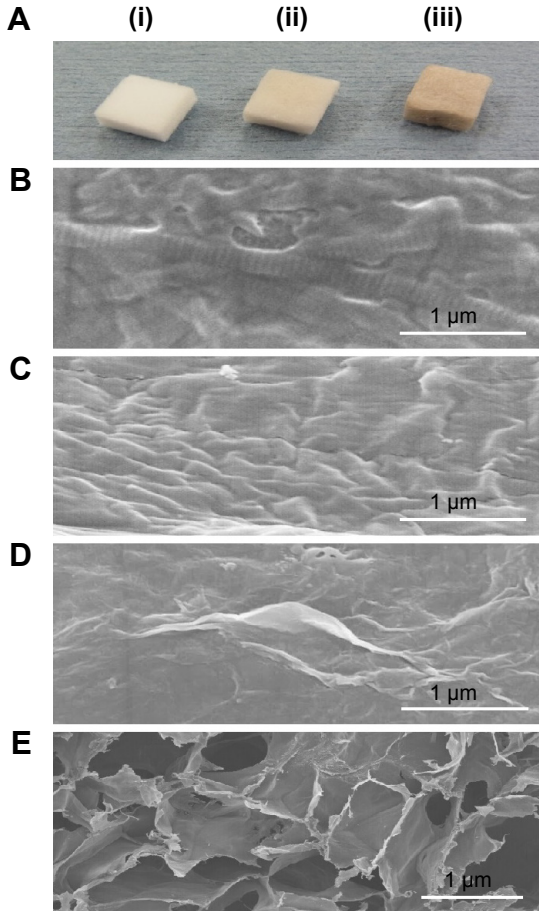

Figure 1 Photographs and SEM images of the collagen scaffolds.
Notes: (**A**) Photographs of the collagen scaffold (i), 0.1 μg/mL GO scaffold (ii), and 1 μg/mL GO scaffold (iii). SEM images of collagen scaffold (**B**), 0.1 μg/mL GO scaffold (**C**), and 1 μg/mL GO scaffold (**D** and **E**). (**D**) The wrinkled structure of GO was observed on collagen fibers. (**E**) GO scaffold possessed an interconnected structure.
Abbreviations: GO, graphene oxide; SEM, scanning electron microscopy.

Characterization of GO scaffold

The GO weight attached to collagen scaffolds was measured. The scaffold porosity was calculated according to the following equation:

$$\text{porosity} = 100 \times \left(1 - \frac{\rho_1}{\rho_2}\right) \quad (1)$$

where ρ_1 denotes the bulk density of the scaffold and ρ_2 signifies the theoretical density. Subsequently, scaffolds were submitted for characterization using a scanning electron microscope (SEM, S-4000; Hitachi Ltd., Tokyo, Japan) with accelerating voltage of 10 kV. The compressive strength of scaffolds was measured using a universal testing machine (EZ-S; Shimadzu Corp., Kyoto, Japan) with a crosshead loading speed of 0.5 mm/min.

In addition, each scaffold was assessed for enzyme degradation and adsorption of Ca and proteins. Preweighed dry scaffolds were immersed for 3 hours at 37°C in phosphate-buffered saline (PBS) with 1% collagenase Type I (Wako Pure Chemical Industries Ltd.). After ethanol dehydration and air-drying, the scaffold weight loss was ascertained. To detect the Ca adsorption capability, each scaffold was immersed in 0.5 mL fetal bovine serum (FBS; Corning Incorporated, Corning, NY, USA) at 37°C. After rinsing several times with PBS, the scaffolds were immersed in 0.5 mL acetic acid for 24 hours at 37°C. The Ca ion content of the supernatant was assessed using a Calcium E-test WAKO (Wako Pure Chemical Industries Ltd.) in accordance with the manufacturer's instructions. To detect the ability of protein adsorption, each scaffold was injected with 100 μL of sterile distilled water (Otsuka Pharmaceutical Co. Ltd., Tokyo, Japan) including 50 μg bovine serum albumin (Wako Pure Chemical Industries Ltd.) or 50 μg lysozyme hydrochloride (from egg white; Wako Pure Chemical Industries Ltd.) under a vacuum condition. Subsequently, the protein-loaded scaffold was placed in 0.9 mL of deionized distilled water. After stirring well, the protein content of the supernatant was assessed using a total protein kit (Micro Lowry, Peterson's Modification; Sigma-Aldrich Co., St Louis, MO, USA) in accordance with the manufacturer's instructions. Then, the amounts of albumin and lysozyme adsorbed onto the scaffold were calculated.

Assessment of GO scaffold cytocompatibility

To evaluate GO scaffold cytocompatibility, 5×10^4 mouse osteoblastic MC3T3-E1 cells (RIKEN BioResource Center, Tsukuba, Japan) were seeded on scaffolds and were cultured in humidified 5% CO_2 at 37°C using minimum essential medium (alpha-GlutaMAX™-I; Thermo Fisher Scientific Inc., Waltham, MA, USA) supplemented with 10% FBS (Qualified; Thermo Fisher Scientific Inc.) and 1% antibiotics (penicillin/streptomycin; Thermo Fisher Scientific Inc.). Cell viability was assessed after 1, 3, 5, and 7 days of culture using a WST-8; cell counting kit-8 (CCK-8; Dojindo Laboratories, Kumamoto, Japan) in accordance with the manufacturer's instructions. The optical density was measured using a microplate reader at 450 nm absorbance.

After 1 day of culture, some samples were fixed in 2.5% glutaraldehyde in 0.1 M sodium cacodylate buffer (pH 7.4) for 30 minutes and were rinsed in cacodylate buffer solution. They were then dehydrated in increasing concentrations of ethanol. Following critical point drying, the specimens were analyzed using SEM. In addition to detection of the in vitro cell ingrowth into the scaffold, some samples cultured for

7 days were embedded in paraffin wax according to the conventional method and were cut into 6 μm thick sections. The sections were stained with hematoxylin–eosin and were observed using light microscopy.

Assessment of rat subcutaneous tissue response to GO scaffold

The experimental protocol followed the institutional animal use and care regulations of Hokkaido University (Animal Research Committee of Hokkaido University, Approval number 13-76). Eighteen 10-week-old male Wistar rats weighing 190–210 g were given general anesthesia by intraperitoneal injection of 0.6 mL/kg sodium pentobarbital (Somnopenthyl; Kyoritsu Seiyaku Corp., Tokyo, Japan) and local injection of 2% lidocaine hydrochloride with 1:80,000 epinephrine (Xylocaine Cartridge for Dental Use; Dentsply Sankin K.K., Tokyo, Japan). After a skin incision was made in the back, each scaffold was implanted into the subcutaneous tissue of the back of each rat. Skin flaps were sutured (Softretch 4-0; GC, Tokyo, Japan). Then, tetracycline hydrochloride ointment (achromycin ointment; POLA Pharma Inc., Tokyo, Japan) was applied to the wound. At 10 and 35 days postsurgery, rats were euthanized using an overdose of sodium pentobarbital (2.0 mL/kg).

To assess the scaffold DNA contents, several specimens extracted from the wound were freeze-dried. Following pulverization, 0.5 mL of 2 M NaCl and 0.05 M phosphate buffer (pH 7.4) were added to each scaffold. After centrifugation, DNA contents of infiltrated cells were examined using a DNA quantification kit (Primary Cell Co. Ltd., Sapporo, Japan) according to the manufacturer's instructions and using a fluorescence spectrophotometer (F-3000; Hitachi Ltd.) at the respective excitation and emission wavelengths of 356 and 458 nm.

Six samples were collected at 10 days for histological observation. The tissue blocks, including the surrounding soft tissue, were fixed in 10% buffered formalin for 24 hours, embedded in paraffin wax according to the conventional method, and cut into 6 μm thick sections. The sections were stained with hematoxylin–eosin and were observed histologically using light microscopy. Histomorphometric measurements of the tissue ingrowth area were taken using software (ImageJ 1.41; National Institutes of Health, Bethesda, MD, USA). In addition, three area units (0.12 mm^2 per unit) at the peripheral area of scaffold were selected under a light microscope. The foreign body giant cells in the unit were counted. These evaluations were assessed using three stained sections: one from the center of the excised tissue sample and one from tissue 1 mm to either side of the center.

Immunohistochemical assessment of implanted GO scaffold

For immunohistochemistry, anesthetized rats were perfused via the aorta with physiological saline, followed by 4% formaldehyde in 0.1 M phosphate buffer, pH 7.4. Tissues were removed, immersed in the same fixative for an additional 24 hours, and dipped in 30% sucrose solution. The tissues were embedded in optimal cutting temperature (OCT) compound (Sakura Finetek Inc., Tokyo, Japan), and were quickly frozen in liquid nitrogen. Frozen sections, approximately 16 μm thick, were mounted on poly-L-lysine-coated glass slides. After pretreatment with 0.3% Triton X-100 and normal donkey serum, the sections were incubated overnight with the following primary antibodies: mouse anti-CD68 (ED-1; 1:100 in dilution; Bio-Rad Laboratories Inc., Hercules, CA, USA), mouse anti-CD163 (ED-2; 1:100 in dilution; Bio-Rad Laboratories Inc.), mouse anti-prolyl-4-hydroxylase beta (P4HB; 1:1,600 in dilution, clone6-9H6; Acris Antibodies, Inc., San Diego, CA, USA), and mouse anti-α-smooth muscle actin (ASMA; 1:1,600 in dilution, clone 1A4; Sigma-Aldrich Co.). The antigen–antibody reaction sites were detected by incubation with Cy3-labeled anti-mouse IgG (Jackson ImmunoResearch Inc., West Grove, PA, USA). Nuclear staining was performed with short incubation (TOTO3; Thermo Fisher Scientific Inc.). The stained sections were mounted with glycerin-PBS and were observed under a confocal laser scanning microscope (Fluoview; Olympus). To detect granulocytes, the sections were incubated in 0.01 M Tris-HCl buffer (pH 7.6) containing 0.01% 3,3′-diaminobenzidine and 0.001% H_2O_2. The specificity of immunoreactions on sections was confirmed according to a conventional procedure. The sections incubated with normal mouse serum instead of respective primary antibody were used as negative controls.

Implantation of GO scaffold to extraction sockets of dogs

Four healthy female beagle dogs, aged 10 months and weighing approximately 9–10 kg, were used for this experiment. Experimental protocols conformed to the institutional animal use and care regulations of Hokkaido University (Approval number 8-255). Surgical procedures were performed under general anesthesia with medetomidine hydrochloride (0.1 mL/kg, Domitor; Nippon Zenyaku Kogyo Co. Ltd., Fukushima, Japan) and butorphanol tartrate (0.1 mL/kg, Vetorphale; Meiji Seika Pharma Co. Ltd., Tokyo, Japan), and under local anesthesia with lidocaine hydrochloride.

Following extraction of maxillar third premolars, scaffold applied with 1 μg/mL GO was embedded into the sockets,

which were then sutured. After 2 weeks, the animals were euthanized using an overdose of sodium pentobarbital (0.5 mL/kg) following general anesthesia with medetomidine hydrochloride (0.1 mL/kg) and butorphanol tartrate (0.1 mL/kg). The tissue blocks, including bone and soft tissue, were fixed in 10% buffered formalin, decalcified in 10% formic–citric acid, and embedded in paraffin wax. We serially prepared 6 μm thick sections along the mesiodistal plane and applied Masson's trichrome staining. Histomorphometric measurements of the rate of bone formation were performed on the center of the excised tissue sample using software (ImageJ 1.41; National Institutes of Health). Radiographic images of extraction sockets were taken immediately following surgery and at 2 weeks after scaffold implantation.

Statistical analysis

The mean and standard deviation of each parameter was calculated for each group. Statistical analysis was performed for each measurement using a Student's *t*-test or Scheffé test. *P*-values <0.05 were inferred as statistically significant. All statistical procedures were done using SPSS 11.0 (IBM Corporation, Armonk, NY, USA).

Results

Characterization of GO scaffold

In SEM images, the GO scaffold rarely showed striations of collagen fibers that were readily visible on the untreated collagen scaffold, even on the central region of the scaffold (Figure 1B and C). In SEM images of 1 μg/mL GO scaffold, we frequently found a wrinkled structure of GO without large aggregate formation (Figure 1D). In fact, the GO scaffold possessed an interconnected structure resembling that of the control (Figure 1E). The GO-applied scaffold porosity was equivalent to that of the control (Table 1).

The compressive strength of 1 μg/mL GO scaffold was approximately 1.7-fold greater than that of the control. The difference was statistically significant. The strength of the 0.1 μg/mL GO scaffold was 1.3-fold greater than that of the control (Figure 2A). A degradation test showed that application of GO to the scaffolds increased its resistance to enzymatic degradation. The decrement in content in 1 μg/mL GO scaffold was 85.5%, which was significantly less than that of the control (Figure 2B). The amount of Ca ion adsorption of scaffold was increased by GO application; the scaffold applied with 1 μg/mL GO was approximately 1.2-fold greater than that of the control (Figure 2C). Protein adsorption tests showed that GO scaffold exhibited considerable amounts of albumin and lysozyme adsorption. Adsorption percentages of albumin and lysozyme of the 1 μg/mL GO scaffold were 88% and 40%, respectively (Figure 2D).

Table 1 Structural parameters of the scaffold (*N*=5, mean ± SD)

Characteristics	Control	0.1 μg/mL GO scaffold	1 μg/mL GO scaffold
GO weight (wt %)	NA	1.83±0.57	2.22±0.71
Porosity (%)	97.63±0.05	97.60±0.08	97.60±0.06

Abbreviations: SD, standard deviation; GO, graphene oxide; NA, not applicable.

Cytocompatibility of GO scaffold

After MC3T3-E1 cell seeding, cell infiltration was clearly demonstrated on the GO-applied scaffold (Figure 3A and B). The SEM images show cell spreading with cell process elongation occurring on the GO-applied collagen fibers (Figure 3C). WST-8 assessment showed that MC3T3-E1 cell proliferation on the scaffold was stimulated in a significant and dose-dependent manner by GO application. At 7 days, cell proliferation of 1 μg/mL GO scaffold was 1.6-fold greater than that of control (Figure 3D).

Rat subcutaneous tissue response to GO scaffold

Histological specimens of control (Figure 4A–C) and 0.1 μg/mL GO scaffolds (Figure 4D–F) revealed that the implanted scaffolds appeared to be compressed physically in the connective tissue and that the cell ingrowth into the scaffold was slight. In contrast, the cell ingrowth, containing fibroblast-like cells, giant cells, and blood vessel-like structures, was remarkable in the 1 μg/mL GO scaffold (Figure 4G–I) when compared to 0.1 μg/mL GO scaffold and control. The number of foreign body giant cells, tissue ingrowth area, and DNA contents of the 1 μg/mL GO scaffold were, respectively, approximately 6.2-, 2.5-, and 1.4-fold greater than those of the control (Figure 4J–L).

Immunohistochemical investigation of GO scaffold

Specimens of GO-applied scaffold obtained at 10 days after implantation revealed that macrophages expressing ED-1 and ED-2 and fibroblasts expressing P4HB were found frequently in the scaffold (Figure 5A–C). Vascular structures formed by ASMA-positive smooth muscle cells were remarkable in the 1 μg/mL GO scaffold, especially at the scaffold periphery (Figure 5D). However, control specimens only slightly exhibited cell ingrowth behavior (Figure 5E–H).

In specimens of the 1 μg/mL GO scaffold at 35 days, ED1-positive macrophages were decreased and ED2-positive macrophages were abundant relative to specimens observed at 10 days (Figure 5I and J). The P4HB-positive cells and

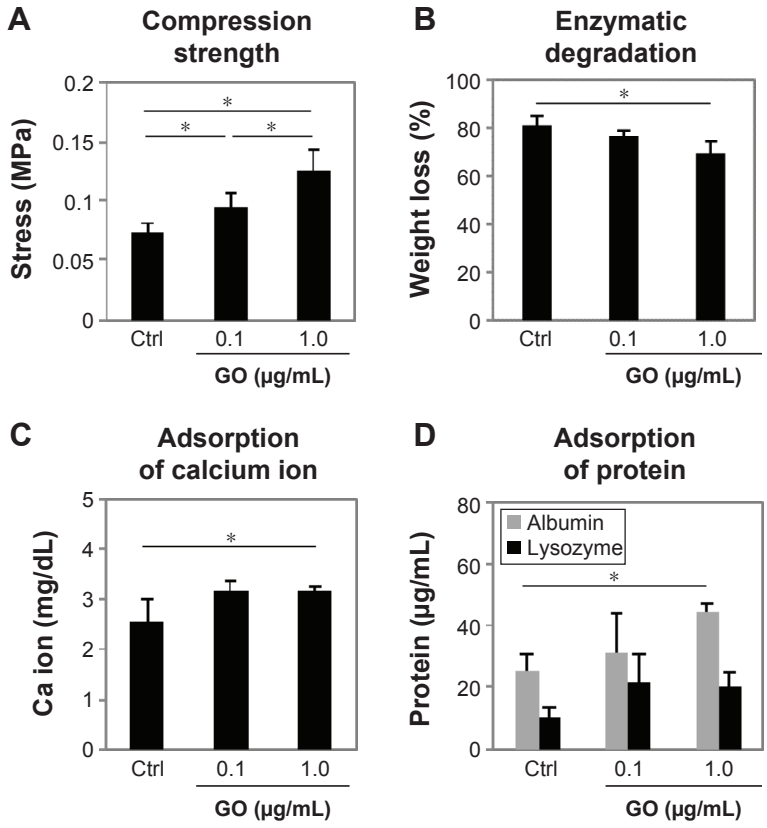

Figure 2 (**A**–**D**) In vitro assessment of each scaffold (*N*=6, mean ± SD).
Note: *$P<0.05$, vs control.
Abbreviations: Crtl, control; GO, graphene oxide; SD, standard deviation.

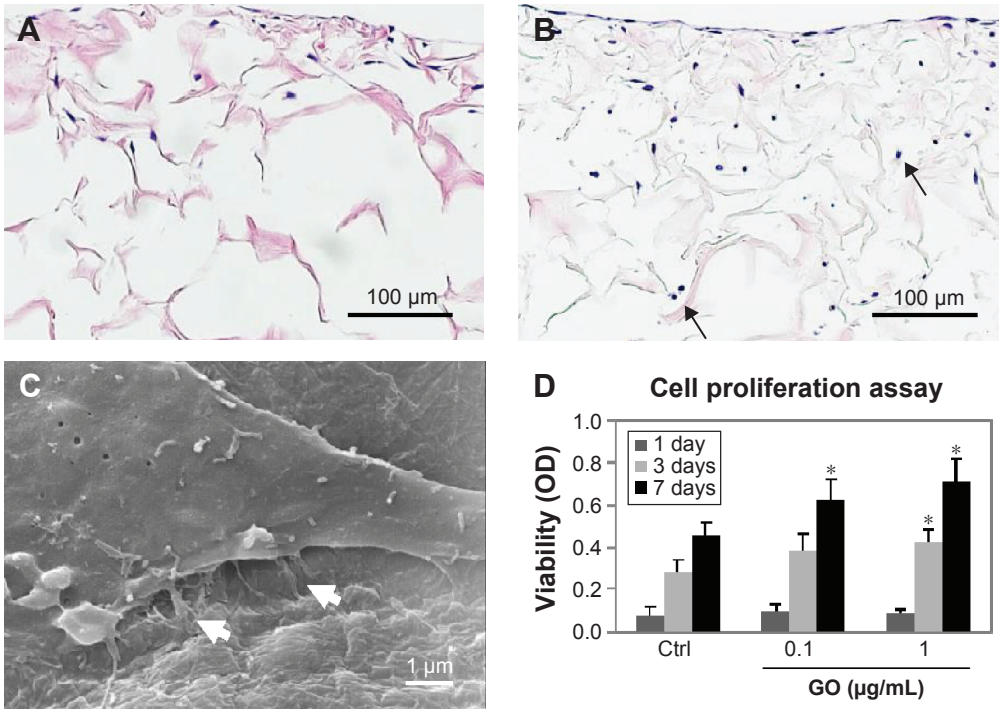

Figure 3 Cytocompatibility of GO scaffold.
Notes: Microscopic images of control (**A**) and 1 μg/mL GO scaffold (**B**) with MC3T3-E1 cells after 7 days incubation. Cultured cells (arrows) were detected frequently in the GO scaffold. (**C**) SEM image of 1 μg/mL GO scaffold with MC3T3-E1 cells after 1 day incubation. Cell spreading with fine processes elongation (white arrows) was observed. (**D**) WST-8 assay (*N*=6, mean ± SD). *$P<0.05$, vs control. Original magnification (**A**, **B**) 25×, (**C**) 10000×.
Abbreviations: Crtl, control; GO, graphene oxide; SEM, scanning electron microscopy; SD, standard deviation.

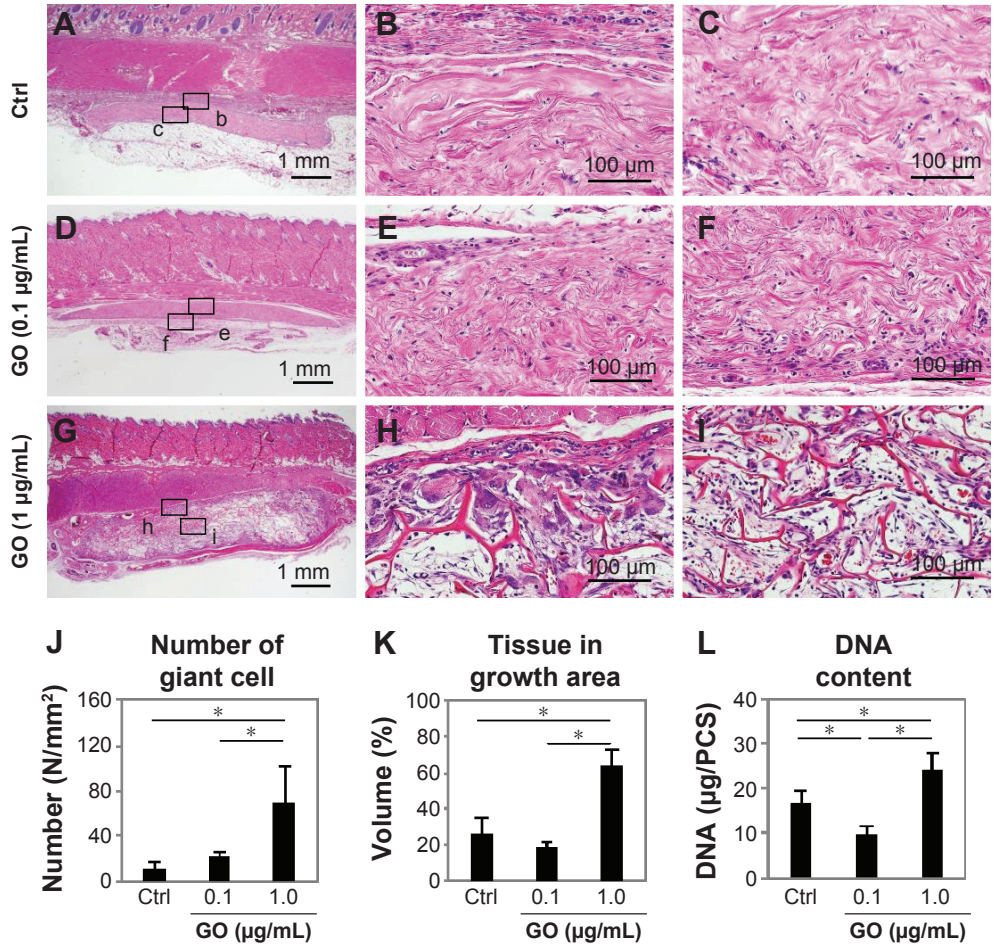

Figure 4 Rat subcutaneous tissue response to GO scaffold.

Notes: Histological findings for control (**A**–**C**), 0.1 μg/mL GO scaffold (**D**–**F**), and 1 μg/mL GO scaffold (**G**–**L**) in rat subcutaneous tissue at 10 days. Rectangles (b, c, e, f, h, and i) in (**A**), (**D**), and (**G**) are enlarged in (**B**), (**C**), (**E**), (**F**), (**H**), and (**I**), respectively. Cell and tissue ingrowth behavior was remarkable in 1 μg/mL GO scaffold. H&E staining. (**J**–**L**) In vivo assessment of each scaffold for number of giant cells, tissue ingrowth area, and DNA content (N=6, mean ± SD). *P<0.05. Original magnification (**A**, **D**, **G**) 3×, (**B**, **C**, **E**, **F**, **H**, **I**) 50×.

Abbreviations: Crtl, control; GO, graphene oxide; H&E, hematoxylin–eosin; SD, standard deviation.

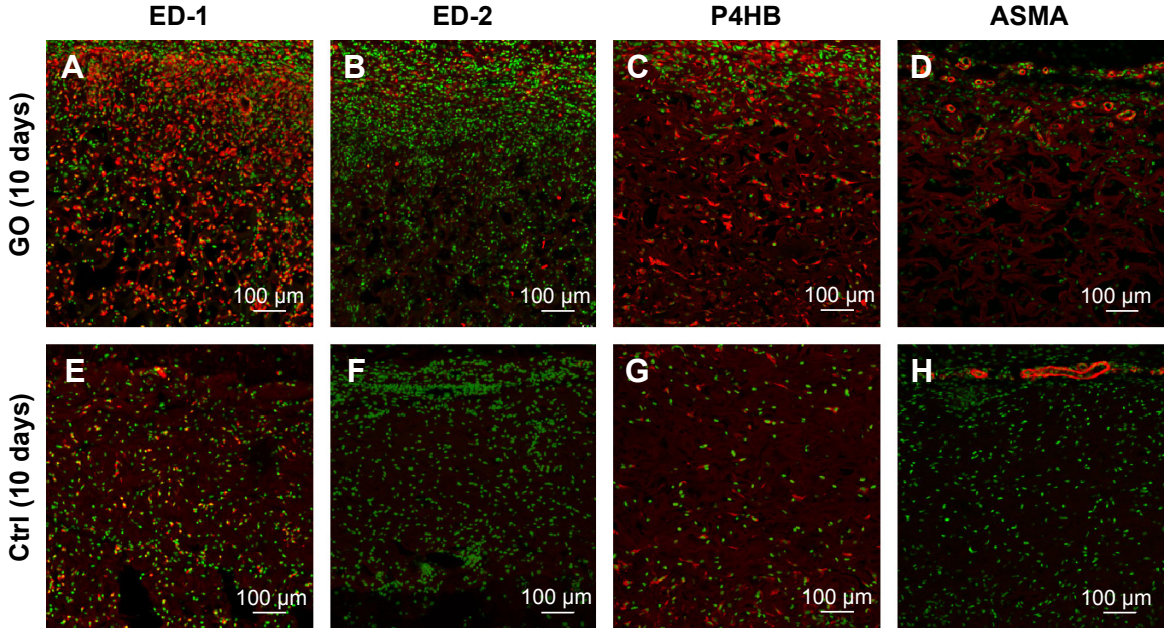

Figure 5 (*Continued*)

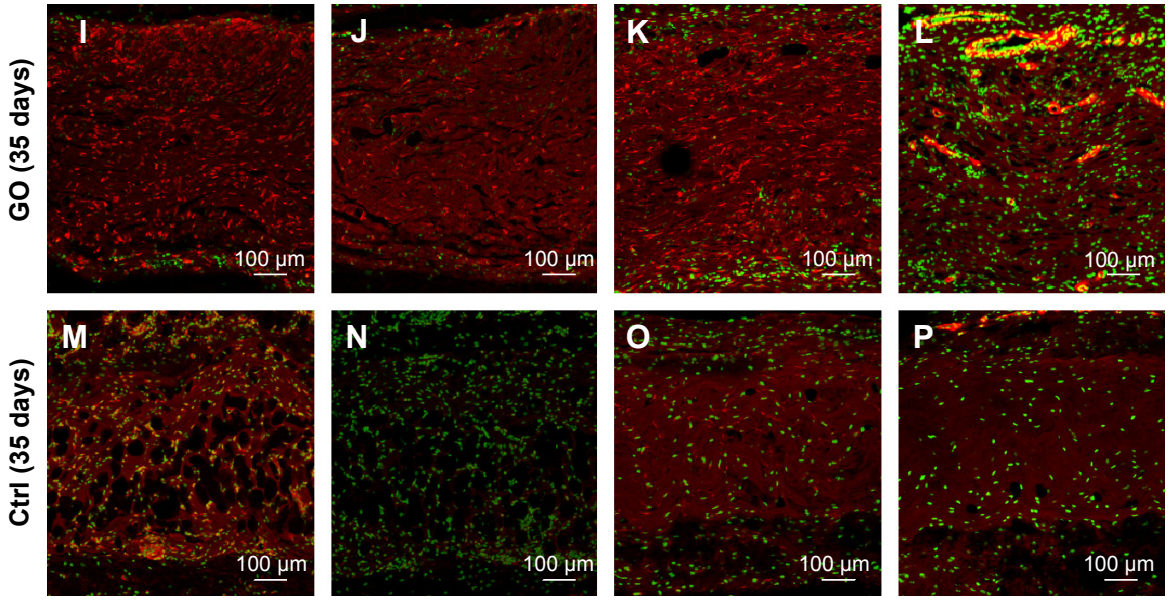

Figure 5 Immunohistochemical observation of GO scaffold.
Notes: Immunofluorescence micrographs of macrophages, fibroblasts, and blood vessel cryostat sections stained (in red) with mouse anti-CD68 (ED-1) (**A**, **E**, **I**, **M**), mouse anti-CD163 (ED-2) (**B**, **F**, **J**, **N**), mouse anti-P4HB (**C**, **G**, **K**, **O**), and mouse ASMA (**D**, **H**, **L**, **P**) for 1 μg/mL GO scaffold (**A**–**D**) and control (**E**–**H**) implanted in rat subcutaneous tissue at 10 days and 1 μg/mL GO scaffold (**I**–**L**) and control (**M**–**P**) at 35 days. Infiltration of ED2-positive cells and ASMA-positive arterioles was more remarkable in the GO scaffold than in the collagen scaffold.
Abbreviations: Crtl, control; GO, graphene oxide; P4HB, prolyl-4-hydroxylase beta; ASMA, anti-α-smooth muscle actin.

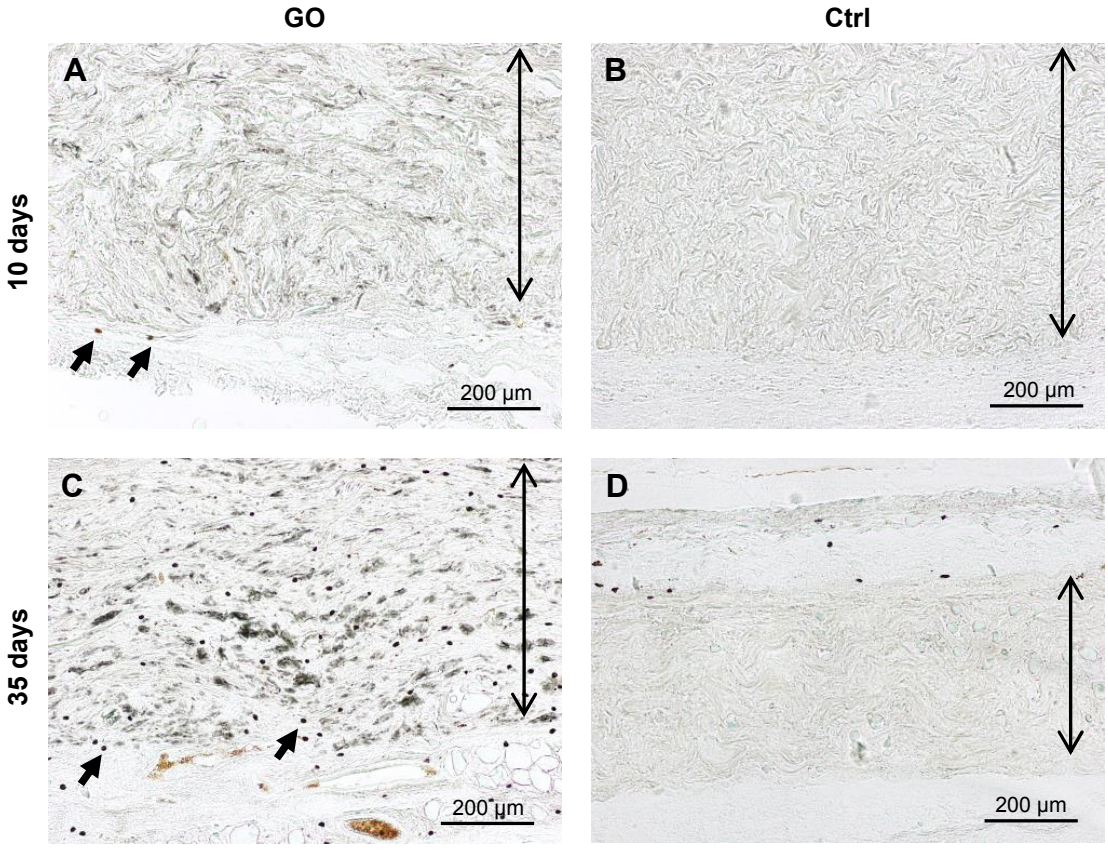

Figure 6 Peroxidase staining of GO scaffold.
Notes: Peroxidase-stained activity for granulocytes in implanted 1 μg/mL GO scaffold (**A**) and control (**B**) in rat subcutaneous tissue at 10 days and 1 μg/mL GO scaffold (**C**) and control (**D**) at 35 days. Peroxidase-positive granulocytes (arrows) were detected slightly around the GO scaffold. Double arrows indicate the implanted scaffold. Original magnification (**A**, **B**, **C**, **D**) 25×.
Abbreviation: GO, graphene oxide.

blood vessels thickened (Figure 5K and L). In control specimens, cell ingrowth behavior at 35 days resembled that in the 10-day specimens (Figure 5M–P).

Peroxidase-positive granulocytes were detected to a slight degree around the 1 μg/mL GO scaffold at 10 and 35 days postsurgery (Figure 6A and C), in contrast to control specimens in which granulocytes were rarely observed (Figure 6B and D).

Implantation of GO scaffold to extraction sockets in dogs

The postoperative healing process appeared to progress well in all four dogs examined (Figure 7A and B). The socket applied with GO scaffold showed increased radiopacity at 2 weeks postsurgery (Figure 7C and D). Histological specimens revealed that GO scaffold application promoted the formation of new bone in the socket (Figure 8A–C). GO aggregation was frequently found in newly formed bone, bone marrow, and connective tissue (Figure 8B and C). New bone formation was slight in the implantation of control scaffold, where most of the socket was filled with connective tissue (Figure 8D and E). The rate of new bone formation in GO-applied specimens was markedly higher than that in control subjects. Mean values for new bone of GO scaffold were approximately fivefold greater than in control (Figure 8F).

Discussion

The results of this study demonstrated that surface modification by GO can provide remarkable bioactivity to 3D scaffolds produced from collagen. Particularly, in vitro cell proliferation was strongly upregulated, as were in vivo cell and blood vessel ingrowth effects. Ordinarily, scaffolds for tissue engineering require exhibition of biocompatible morphology and properties, as well as porous structure and physical strength.[37] In addition, the surface morphology of

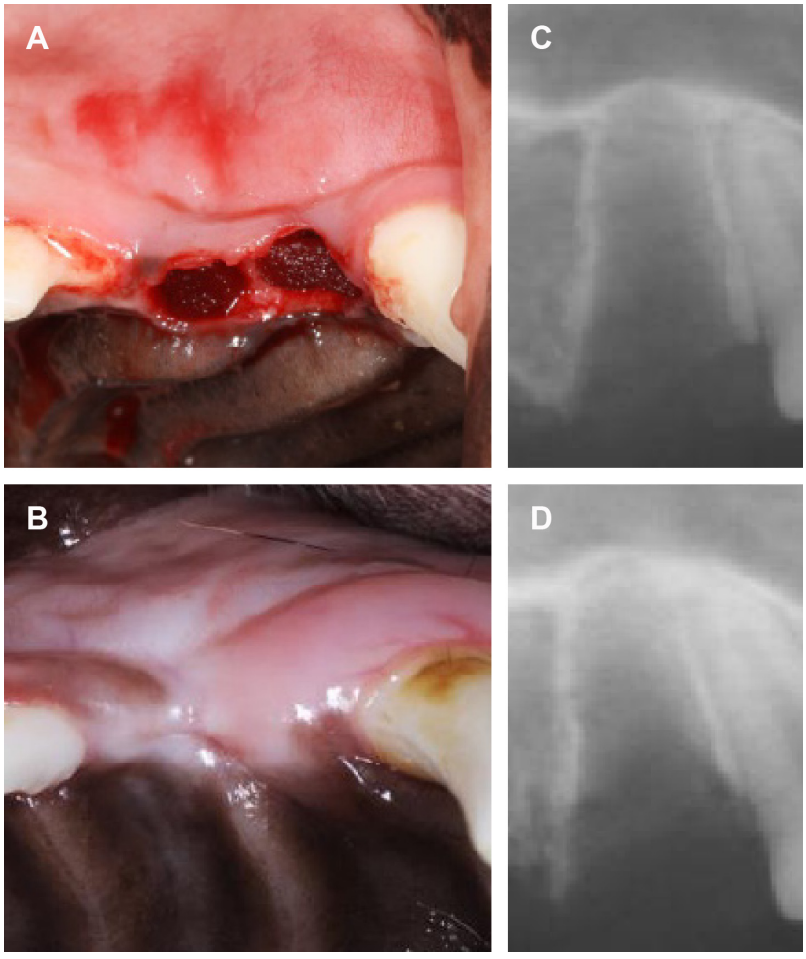

Figure 7 Implantation of GO scaffold to extraction socket.
Notes: (**A**) Photograph of implanted scaffold. (**B**) Macroscopic view at 2 weeks postsurgery. (**C**) Radiographic images immediately after operations. (**D**) Radiographic image at 2 weeks postsurgery. The socket applied with GO scaffold showed increased radiopacity.
Abbreviation: GO, graphene oxide.

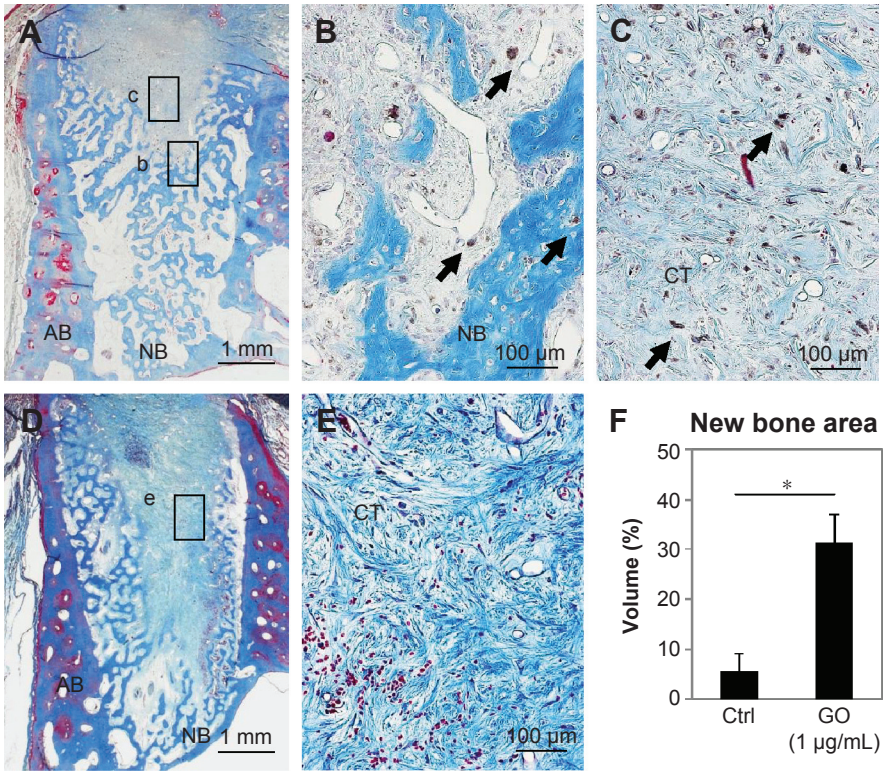

Figure 8 Histological findings in extraction socket at 2 weeks.
Notes: (**A**) Specimen receiving 1 μg/mL GO scaffold. (**B** and **C**) Higher magnification of the framed area (b, c) in (**A**). Residual GO (arrows) were observed in newly formed bone and connective tissue. (**D**) Specimen receiving control material. (**E**) Higher magnification of the framed area (e) in (**D**). MT staining. (**F**) Histomorphometric measurements of newly formed area. *$P<0.05$. Original magnification (**A**, **D**) 3×, (**B**, **C**, **E**) 50×.
Abbreviations: AB, alveolar bone; NB, new bone; CT, connective tissue; GO, graphene oxide; MT, Masson's trichrome; Crtl, control.

the interface between cells and biomaterials strongly affects the cell behavior in terms of cell migration, proliferation, and differentiation.[38,39] The application of nanoparticle-modified structures might increase the surface area and subsequent signaling molecule adsorption, thereby improving cell behaviors.[10–12,40] The present SEM observation in 1 μg/mL GO scaffold demonstrated that wrinkling structures covered by GO sheets were formed frequently on the collagen strut of the scaffold. The GO sheet possesses many functional groups including hydroxyl (OH), epoxy (C–O–C), and carboxyl (COOH) species on its surface. Therefore, GO can adsorb some biomolecules to improve their chemical and biological properties.[41] In fact, GO-applied scaffold was able to adsorb both acidic protein (albumin) and basic protein (lysozyme) in the protein adsorption test. Therefore, various biological molecules supplied by FBS can be retained on the GO surface and can provide cytocompatibility effects for MC3T3-E1 cell infiltration and proliferation in the scaffold. Ryoo et al[42] reported that focal adhesion of NIH-3T3 fibroblastic cells on the GO substrate surface was promoted and that an attachment protein, vinculin, was expressed abundantly on the cells by the GO. They thus concluded that the GO surface is biocompatible.

Actually, GO application stimulated cell and tissue ingrowth in rat subcutaneous tissues. Macrophages are known to secrete various cytokines that stimulate granulation tissue formation and that frequently reconstruct bone tissue.[43] Immunohistochemical assessment of 1 μg/mL GO scaffolds at 10 and 35 days after implantation revealed enhanced infiltration of macrophages expressing ED-1, fibroblasts expressing P4HB, and neutrophils in the scaffold. That result suggests that GO induces scaffold degradation, reflecting phagocytosis by macrophages, and that it causes the subsequent production of extracellular matrix such as collagen. Furthermore, the 1 μg/mL GO scaffold actively caused formation of blood vessels, including arterioles with ASMA-positive smooth muscle cells. Consequently, GO application is expected to stimulate angiogenesis to provide oxygen and nutrition for tissue remodeling. Lucas et al[44] reported that activated macrophages controlled the natural sequence of repair event in wound healing. Activated macrophages are classified into activated macrophages (M1 macrophage) and wound-healing macrophages (M2 macrophage). The latter are associated with immunosuppression and with tissue repair and remodeling, playing critical roles in the resolution of inflammatory responses.[45,46] In this study, ED2-positive

M2 macrophages were remarkably abundant in 1 μg/mL GO scaffold at 10 and 35 days postsurgery in contrast to the control material, which scarcely contained ED2-positive macrophages, suggesting that GO application to the scaffold enhances tissue repair via macrophage recruitment.

The examinations of the physical properties of the scaffold presented herein revealed that GO application reinforced compressive strength and collagenase resistance by the wrapping of scaffold collagen fibers with GO nanofilms and by the deep infiltration of GO into collagen scaffold. The GO coating layer has been shown to enhance the collagen scaffold stability because of attractive force attributable to its nanoscale distance.[47] In bone regenerative therapy, the mechanical stiffness of the scaffold played an important role in maintaining a tissue-reconstructive inner space for osteogenic cells such as osteoblasts.[48] Although regenerative scaffolds should be designed to provide a highly porous structure for stimulating tissue ingrowth, higher porosity generally causes lower mechanical strength.[49] In this study, the GO scaffold porosity was equivalent to that of control materials. A SEM image of the 1 μg/mL GO revealed an interconnected porous structure with high porosity. Therefore, regenerative cells were able to infiltrate into the scaffold. In histological findings of rat subcutaneous tissue, 1 μg/mL GO scaffold maintained space for tissue reconstruction. Moreover, the 0.1 μg/mL GO scaffold was compressed as in the control. Although a previous study revealed that high-dose application of GO (10 μg/mL) to the scaffold strongly promoted the scaffold mechanical strength, it also inhibited cell infiltration into the scaffold.[28] Wang et al[33] reported that GO exhibited remarkable cytotoxicity that included decreasing cell adhesion and induction of cell apoptosis. GO induced the production of reactive oxygen species (ROS) to decrease cell viability.[50] Therefore, it seems likely that ROS production resulting from an overdose of GO increases cytotoxicity. In vivo degradation of scaffold applied with 10 μg/mL GO was inactive,[28] suggesting that its residue remained in the tissue for a long time and that exposure of the residue increased the risk of infection and inhibitory effects on tissue engineering. Accordingly, we speculate that GO application at low doses (1 μg/mL) eliminated adverse effects of ROS and stimulated tissue response as a catalytic effect.

Bone formation assessment of dog extraction sockets revealed that providing a GO scaffold promoted bone induction significantly, suggesting that GO scaffold had positive effects on osteoblastic cell responses in addition to improving their physical properties. On the basis of the results of subcutaneous experiments in rats, GO scaffold was found to conceivably guide cells of various types related to bone induction from tissues surrounding the extraction socket. Subsequently, the production of extracellular matrix and circulation induced by angiogenesis might occur in the GO scaffold. Early regenerative tissue accumulation might precede epithelial tissue invasion into the socket. An earlier study revealed that GO application enhanced the bioactivities of bone marrow stromal cells, such as proliferation, alkaline phosphatase activity, and expression of Wnt signaling pathway associated with osteogenic differentiation.[30] In addition, many functional groups on the GO surface are well suited to interaction with cations and anions, thereby enhancing Ca adsorption.[41,51,52] We speculate that the Ca adsorption of GO scaffold was enhanced by graphite intercalation, ie, insertion of Ca between GO nanolayers. Results show that Ca ion stimulated the expression of osseous markers in osteoblastic cells, stimulated alkaline phosphatase activity, and adjusted the in vivo environment for bone generation.[53,54] As demonstrated in this study, Ca accumulation on the surface of GO scaffold might provide a favorable environment for bone tissue formation. It is expected that GO scaffold is beneficial for future clinical applications in the disease models such as periodontal disease and bone metastasis. Further studies are necessary to assess the potential for osseous regeneration and augmentation of GO scaffolds.

Conclusion

Effects of GO application to a 3D collagen scaffold were examined in vitro and in vivo. The results show that GO application improved the physical properties of collagen scaffold, such as compressive strength, enzyme resistance, and adsorption of Ca and proteins. Osteoblastic MC3T3-E1 cell proliferation was remarkable on the GO-applied scaffold. In addition, GO application stimulated biological effects. Particularly, scaffold applied with 1 μg/mL GO remarkably induced cell and tissue ingrowth behavior as well as angiogenesis in rat subcutaneous tissues. In the extraction sockets of dogs, GO scaffold exhibited approximately fivefold increased bone formation when compared to the collagen scaffold. These results suggest that GO provided biocompatibility and high bone-forming capability for the scaffold. Therefore, GO scaffolds are expected to be useful and beneficial for bone tissue engineering therapy.

Acknowledgments

The authors thank Mitsubishi Gas Chemical Co. Inc. for providing nanoGRAX® and Olympus Terumo Biomaterials Corp. for providing collagen scaffolds. This work was supported by JSPS KAKENHI Grant Numbers 25463210 and 26870016.

Disclosure

The authors report no conflicts of interest in this work.

References

1. Yang S, Leong KF, Du Z, Chua CK. The design of scaffolds for use in tissue engineering. Part I. Traditional factors. *Tissue Eng*. 2001;7(6):679–689.
2. Chen FM, Jin Y. Periodontal tissue engineering and regeneration: current approaches and expanding opportunities. *Tissue Eng Part B Rev*. 2010;16(2):219–255.
3. Li WJ, Tuli R, Huang X, Laquerriere P, Tuan RS. Multilineage differentiation of human mesenchymal stem cells in a three-dimensional nanofibrous scaffold. *Biomaterials*. 2005;26(25):5158–5166.
4. Hutmacher DW. Scaffolds in tissue engineering bone and cartilage. *Biomaterials*. 2000;21(24):2529–2543.
5. Lutolf MP, Hubbell JA. Synthetic biomaterials as instructive extracellular microenvironments for morphogenesis in tissue engineering. *Nat Biotechnol*. 2005;23(1):47–55.
6. Teng YD, Lavik EB, Qu X, et al. Functional recovery following traumatic spinal cord injury mediated by a unique polymer scaffold seeded with neural stem cells. *Proc Natl Acad Sci U S A*. 2002;99(5):3024–3029.
7. Kim S, Kim SS, Lee SH, et al. In vivo bone formation from human embryonic stem cell-derived osteogenic cells in poly(D, L-lactic-co-glycolic acid)/hydroxyapatite composite scaffolds. *Biomaterials*. 2008;29(8):1043–1053.
8. Zhou W, Zhong X, Wu X, et al. The effect of surface roughness and wettability of nanostructured TiO_2 film on TCA-8113 epithelial-like cells. *Surf Coat Technol*. 2006;200(20–21):6155–6160.
9. Rosales-Leal JI, Rodríguez-Valverde MA, Mazzaglia G, et al. Effect of roughness, wettability and morphology of engineered titanium surfaces on osteoblast-like cell adhesion. *Colloid Surf A*. 2010;365(1–3):222–229.
10. Thapa A, Miller DC, Webster TJ, Haberstroh KM. Nano-structured polymers enhance bladder smooth muscle cell function. *Biomaterials*. 2003;24(17):2915–2926.
11. Huang HH, Ho CT, Lee TH, Lee TL, Liao KK, Chen FL. Effect of surface roughness of ground titanium on initial cell adhesion. *Biomol Eng*. 2004;21(3–5):93–97.
12. Zhang L, Ramsaywack S, Fenniri H, Webster TJ. Enhanced osteoblast adhesion on self-assembled nanostructured hydrogel scaffolds. *Tissue Eng Part A*. 2008;14(8):1353–1364.
13. Usui Y, Aoki K, Narita N, et al. Carbon nanotubes with high bone-tissue compatibility and bone-formation acceleration effects. *Small*. 2008;4(2):240–246.
14. Han ZJ, Rider AE, Ishaq M, et al. Carbon nanostructures for hard tissue engineering. *RSC Adv*. 2013;3:11058–11072.
15. Kasai T, Matsumura S, Iizuka T, et al. Carbon nanohorns accelerate bone regeneration in rat calvarial bone defect. *Nanotechnology*. 2011;22(6):065102.
16. Elias KL, Price RL, Webster TJ. Enhanced functions of osteoblasts on nanometer diameter carbon fibers. *Biomaterials*. 2002;23:3279–3287.
17. Chen GY, Pang DWP, Hwang SM, Tuan HY, Hu YC. A graphene-based platform for induced pluripotent stem cells culture and differentiation. *Biomaterials*. 2012;33:418–427.
18. Tang M, Song Q, Li N, Jiang Z, Huang R, Cheng G. Enhancement of electrical signaling in neural networks on graphene films. *Biomaterials*. 2013;34:6402–6411.
19. Dikin DA, Stankovich S, Zimney EJ, et al. Preparation and characterization of graphene oxide paper. *Nature*. 2007;448(7152):457–460.
20. Dreyer DR, Park S, Bielawski CW, Ruoff RS. The chemistry of graphene oxide. *Chem Soc Rev*. 2010;39(1):228–240.
21. Marcano DC, Kosynkin DV, Berlin JM, et al. Improved synthesis of graphene oxide. *ACS Nano*. 2010;4(8):4806–4814.
22. Sun X, Liu Z, Welsher K, et al. Nano-graphene oxide for cellular imaging and drug delivery. *Nano Res*. 2008;1(3):203–212.
23. Sayyar S, Murray E, Thompson BC, Gambhir S, Officer DL, Wallace GG. Covalently linked biocompatible graphene/polycaprolactone composites for tissue engineering. *Carbon*. 2013;52:296–304.
24. La WG, Park S, Yoon HH, et al. Delivery of a therapeutic protein for bone regeneration from a substrate coated with graphene oxide. *Small*. 2013;9(23):4051–4060.
25. Qin W, Li X, Bian WW, Fan XJ, Qi JY. Density functional theory calculations and molecular dynamics simulations of the adsorption of biomolecules on graphene surfaces. *Biomaterials*. 2010;31(5):1007–1016.
26. Goenka S, Sant V, Sant S. Graphene-based nanomaterials for drug delivery and tissue engineering. *J Control Release*. 2014;173:75–88.
27. Lee WC, Lim CH, Tang LA, et al. Origin of enhanced stem cell growth and differentiation on graphene and graphene oxide. *ACS Nano*. 2011;5(9):7334–7341.
28. Nishida E, Miyaji H, Takita H, et al. Graphene oxide coating facilitates the bioactivity of scaffold material for tissue engineering. *Jpn J Appl Phys*. 2014;53(6S):06JD04.
29. Dinescu S, Ionita M, Pandele AM, et al. In vitro cytocompatibility evaluation of chitosan/graphene oxide 3D scaffold composites designed for bone tissue engineering. *Biomed Mater Eng*. 2014;24(6):2249–2256.
30. Wu C, Xia L, Han P, et al. Graphene-oxide-modified β-tricalcium phosphate bioceramics stimulate in vitro and in vivo osteogenesis. *Carbon*. 2015;93:116–129.
31. Huang J, Best SM, Bonfield W, et al. In vitro assessment of the biological response to nano-sized hydroxyapatite. *J Mater Sci Mater Med*. 2004;15(4):441–445.
32. Bottini M, Bruckner S, Nika K, et al. Multi-walled carbon nanotubes induce T lymphocyte apoptosis. *Toxicol Lett*. 2006;160(2):121–126.
33. Wang K, Ruan J, Song H, et al. Biocompatibility of graphene oxide. *Nanoscale Res Lett*. 2011;6(8):1.
34. Liao KH, Lin YS, Macosko CW, Haynes CL. Cytotoxicity of graphene oxide and graphene in human erythrocytes and skin fibroblasts. *ACS Appl Mater Interfaces*. 2011;3:2607–2615.
35. Hummers WS Jr, Offeman RE. Preparation of graphitic oxide. *J Am Chem Soc*. 1958;80(6):1339.
36. Hirata M, Gotou T, Horiuchi S, Fujiwara M, Ohba M. Thin-film particles of graphite oxide 1: high-yield synthesis and flexibility of the particles. *Carbon*. 2004;42(14):2929–2937.
37. Salgado AJ, Coutinho OP, Reis RL. Bone tissue engineering: state of the art and future trends. *Macromol Biosci*. 2004;4:743–765.
38. Ibara A, Miyaji H, Fugetsu B, et al. Osteoconductivity and biodegradability of collagen scaffold coated with nano-β-TCP and fibroblast growth factor 2. *J Nanomater*. 2013;2013:46.
39. Yoshida T, Miyaji H, Otani K, et al. Bone augmentation using a highly porous PLGA/β-TCP scaffold containing fibroblast growth factor-2. *J Periodont Res*. 2015;50:265–273.
40. Miyaji H, Sugaya T, Ibe K, Ishizuka R, Tokunaga K, Kawanami M. Root surface conditioning with bone morphogenetic protein-2 facilitates cementum-like tissue deposition in beagle dogs. *J Periodont Res*. 2010;45(5):658–663.
41. Li M, Wang Y, Liu Q, et al. In situ synthesis and biocompatibility of nano hydroxyapatite on pristine and chitosan functionalized graphene oxide. *J Mater Chem B*. 2013;1:475–484.
42. Ryoo SR, Kim YK, Kim MH, Min DH. Behaviors of NIH-3T3 fibroblasts on graphene/carbon nanotubes: proliferation, focal adhesion, and gene transfection studies. *ACS Nano*. 2010;4(11):6587–6598.
43. Kim YH, Furuya H, Tabata Y. Enhancement of bone regeneration by dual release of a macrophage recruitment agent and platelet-rich plasma from gelatin hydrogels. *Biomaterials*. 2014;35:214–224.
44. Lucas T, Waisman A, Ranjan R, et al. Differential roles of macrophages in diverse phases of skin repair. *J Immunol*. 2010;184(7):3964–3977.
45. Mantovani A, Biswas SK, Galdiero MR, Sica A, Locati M. Macrophage plasticity and polarization in tissue repair and remodeling. *J Pathol*. 2013;229(2):176–185.

46. Ito T, Kaneko T, Yamanaka Y, Shigetani Y, Yoshiba K, Okiji T. M2 macrophages participate in the biological tissue healing reaction to mineral trioxide aggregate. *J Endod*. 2014;40(3):379–383.
47. Kanayama I, Miyaji H, Takita H, et al. Comparative study of bioactivity of collagen scaffolds coated with graphene oxide and reduced graphene oxide. *Int J Nanomed*. 2014;9(1):3363–3373.
48. Liu X, Smith LA, Hu J, Ma PX. Biomimetic nanofibrous gelatin/apatite composite scaffolds for bone tissue engineering. *Biomaterials*. 2009;30:2252–2258.
49. Karageorgiou V, Kaplan D. Porosity of 3D biomaterial scaffolds and osteogenesis. *Biomaterials*. 2005;26:5474–5491.
50. Chang Y, Yang ST, Liu JH, et al. In vitro toxicity evaluation of graphene oxide on A549 cells. *Toxicol Lett*. 2011;200(3):201–210.
51. Depan D, Girase B, Shah JS, Misra RD. Structure–process–property relationship of the polar graphene oxide-mediated cellular response and stimulated growth of osteoblasts on hybrid chitosan network structure nanocomposite scaffolds. *Acta Biomater*. 2011;7:3432–3445.
52. Girase B, Shah JS, Misra RDK. Cellular mechanics of modulated osteoblasts functions in graphene oxide reinforced elastomers. *Adv Eng Mater*. 2012;14(4):B101–B111.
53. Sugimoto T, Kanatani M, Kano J, et al. Effects of high calcium concentration on the functions and interactions of osteoblastic cells and monocytes and on the formation of osteoclast-like cells. *J Bone Miner Res*. 1993;8:1445–1452.
54. Lü LX, Zhang XF, Wang YY, et al. Effects of hydroxyapatite-containing composite nanofibers on osteogenesis of mesenchymal stem cells in vitro and bone regeneration in vivo. *ACS Appl Mater Interfaces*. 2013;5:319–330.